Published in final edited form as:
Finite Elem Anal Des. 2011 October 1; 47(10): 1178–1185. doi:10.1016/j.finel.2011.05.007.

Automated subject-specific, hexahedral mesh generation via image registration

Songbai Ji[a,*], **James C. Ford**[b], **Richard M. Greenwald**[a,c], **Jonathan G. Beckwith**[c], **Keith D. Paulsen**[a,d], **Laura A. Flashman**[b], and **Thomas W. McAllister**[b]

[a] Thayer School of Engineering, Dartmouth College, Hanover, NH, USA

[b] Department of Psychiatry, Dartmouth Medical School, Lebanon, NH, USA

[c] Simbex, Lebanon, NH, USA

[d] Norris Cotton Cancer Center, Lebanon, NH, USA

Abstract

Generating subject-specific, all-hexahedral meshes for finite element analysis continues to be of significant interest in biomechanical research communities. To date, most automated methods "morph" an existing atlas mesh to match with a subject anatomy, which usually result in degradation in mesh quality because of mesh distortion. We present an automated meshing technique that produces satisfactory mesh quality and accuracy without mesh repair. An atlas mesh is first developed using a script. A subject-specific mesh is generated with the same script after transforming the geometry into the atlas space following rigid image registration, and is transformed back into the subject space. By meshing the brain in 11 subjects, we demonstrate that the technique's performance is satisfactory in terms of both mesh quality (99.5% of elements had a scaled Jacobian >0.6 while <0.01% were between 0 and 0.2) and accuracy (average distance between mesh boundary and geometrical surface was 0.07 mm while <1% greater than 0.5mm). The combined computational cost for image registration and meshing was <4 min. Our results suggest that the technique is effective for generating subject-specific, all-hexahedral meshes and that it may be useful for meshing a variety of anatomical structures across different biomechanical research fields.

Keywords

subject-specific; automatic mesh generation; hexahedral; mesh quality; finite element analysis; traumatic brain injury; biomechanics; mutual information

1. Introduction

The finite element (FE) method is an effective and widely employed numerical technique for simulating responses of a variety of biological tissues and structures in a broad spectrum of biomechanical engineering applications where physically based experiments are often otherwise infeasible or unethical to perform. The success of this method depends on the

[*]Corresponding author: Songbai Ji, Thayer School of Engineering, Dartmouth College, Hanover, NH 03766, Songbai.Ji@Dartmouth.EDU, Phone: (603) 646-9193, Fax: (603) 646-3699.

geometrical fidelity of the FE model that represents the anatomy of interest and the accuracy of constitutive material properties used to characterize the tissue mechanical behavior, as well as the boundary conditions. To obtain reliable and realistic simulations with sufficient accuracy, detailed and sophisticated FE models have been developed to represent geometrically complex anatomies. These models are often developed from medical images, in which the anatomy of interest is first segmented to define a geometrical surface and an FE model is then derived through a meshing software package [1].

Although tetrahedral elements have commonly been used in biomechanical applications because automated meshing techniques are available, hexahedral elements offer attractive numerical properties relative to tetrahedrons [2]. For example, linear tetrahedral elements tend to be overly stiff and can be susceptible to shear-lock (i.e., spurious shear strains that do not physically exist). In addition, solutions computed on these elements can be slow convergence with mesh refinement [3]. By contrast, linear hexahedral elements are more accurate in nonlinear or impact contact analysis and according to [3] are even more efficient than second order tetrahedrons. However, algorithms to generate hexahedral meshes automatically are still lacking and manual operations are usually involved, which are not only tedious and time consuming but also make subject-specific mesh generation a challenge. Consequently, models based on a generic or average anatomy are often employed in FE studies. Although they have been used successfully to perform realistic global simulations and answer many scientific questions especially in parametric studies (e.g., [4], [5]), they do not capture differences in anatomical morphology or biomechanical properties between individuals. Consequently, these models are limited in individual-subject studies and they do not allow investigations of inter-subject variations.

As a result, subject-specific FE models have gained popularity in a variety of biomechanical research settings (e.g., for the head [6], blood vessels [7], bones [8], heart [9], skeletal muscles [10], teeth [11], and tumors [12]; see [13] for a recent review on current progress in subject-specific modeling). Because subject-specific models are based on individualized instead of average data, they offer a direct link between the FE simulation response (e.g., stress and/or strain) and data obtained from subject-specific imaging studies (e.g., change in fractional anisotropy in diffusion tensor imaging (DTI) that may be an indication of white matter integrity; see, e.g., [14]).

Currently, a barrier to subject-specific modeling appears to be the large number of manual steps involved in the processing from data acquisition to model results [13]. To address the need for generating subject-specific models, a number of algorithms have been developed to facilitate and streamline the process. These techniques are often based on “mesh-matching” methods that essentially register an atlas mesh with the subject-specific anatomical geometry [5, 6, 8, 15, 16, 17, 18]. The atlas mesh is typically constructed manually or semi-manually from a generic anatomy to ensure mesh quality. Once the atlas mesh is available, a subject-specific mesh can be generated automatically by registering the atlas mesh directly to the subject-specific geometry. Although these morphing methods maintain the same mesh topology and density (i.e., the number of nodes and elements and their connectivity remains the same), degradation in mesh quality (or even mesh invalidation, e.g., introduction of inverted elements with negative volumes) can occur because of excessive mesh distortion. Mesh repair is typically algorithmically complicated and time-consuming to perform [18].

Automatic “wrapping” can also be used to match both the atlas and subject-specific anatomical surfaces to an auxiliary surface [16]. However, this technique does not guarantee point-to-point correspondence between the atlas and subject anatomical surfaces and can lead to distorted meshes in small, convoluted regions. Landmarks can be placed on the atlas

and subject-specific surfaces to avoid mesh distortion [16], but requires manual effort and the surface agreement can be poor in regions distant from the landmarks.

To help satisfy the growing need to generate individualized FE models efficiently, we present a technique that produces a subject-specific mesh automatically without degradation in mesh quality or geometrical accuracy. The method matches the atlas *geometry* (as opposed to the atlas mesh) with that of the subject using image-based rigid registration prior to mesh generation. Because mesh distortion is not involved, mesh repair is not necessary. The technique is also applicable to a broad range of anatomical structures because no restriction on the anatomical morphology is imposed, making it attractive for use in a variety of biomechanical settings where subject-specific, hexahedral FE models are desired.

2. Materials and Methods

An effective subject-specific meshing scheme was developed based on a meshing script and rigid image-registration (see Fig. 1 for illustration of the overall scheme). Like other morphing methods, our subject-specific mesh generator requires an atlas mesh to be created. In this study, the atlas mesh was formed from surface geometry derived from the segmented anatomy of interest using a meshing script with a commercial software package (see, e.g., [19] and [20] for exemplified meshing of the femur and heart ventricle, respectively). To generate a subject-specific, hexahedral mesh, the corresponding subject MR image volume is rigidly registered with the atlas by maximizing their mutual information (MI; [21]). The anatomical surface of the subject (subject geometry) is subsequently transformed into the atlas coordinate system (intermediate geometry) to guide execution of the meshing script. The resulting mesh (intermediate mesh) is rigidly transformed back into the subject coordinate system (i.e., subject mesh).

To demonstrate the utility of the technique, we generated subject-specific meshes of the brain in eleven individuals (N=11; 9 males and 2 females) identified with a concussion sustained while playing football or ice hockey. These subjects are part of an ongoing prospective study of the biomechanical basis of concussion in high school and college student athletes who wear instrumented helmets (HIT System [22]) and undergo neuroimaging pre- and post-season, and within two weeks of a concussion (if applicable). All subjects had high-resolution, T1-weighted MR images of the head (16-bit grayscale; 256 × 140 × 256; image resolution 1.0 × 1.2 × 1.0 mm). In order to develop an atlas mesh, we selected a subject whose MR images were approximately symmetrical in the axial plane and we generated subject-specific, hexahedral meshes for the remainder of the subjects (N=10).

2.1 Meshing software

A parametric meshing software package, TrueGrid® (version 2.3; XYZ Scientific Applications Inc., Livermore, CA), was used. This software can be executed either interactively through its graphical user interface or via a script file. Executing a pre-programmed, text-based script file eliminates the need for any user interaction, which maintains the automatic feature of the subject-specific mesh generation technique described in this work.

The meshing software uses a multi-block approach to map highly controllable hexahedral meshes to a geometrical surface and subsequently subdivides the multi-block into hexahedral elements. It projects the boundaries of these building blocks to conform the mesh to a given geometry. In this paper, we used a relatively simple topology for meshing the atlas brain and focused our efforts on the meshing scheme for automating the subject-specific mesh generation.

2.2 Mesh construction for the atlas geometry

The brain was segmented from the atlas MR using FSL (Version 4.1.5; [23]) software and a triangulated iso-surface was generated with an in-house MATLAB routine (R2009b; The Mathworks, Natick, MA). The brain surface was further smoothed and imported into TrueGrid® as a polygonal viewpoint surface to guide the mesh construction (Fig. 2b).

A multi-block was created with its size and position determined by the imported surface. Unnecessary corner blocks were removed to utilize the "butterfly" topology (i.e., portions of the blocks were collapsed and the corresponding exposed nodes along the boundaries were projected to the same physical location; e.g., points with identical labels in Fig. 3a; [24]) in order to avoid degradation in mesh quality when mesh density increases. The corner nodes were *not* projected to the brain surface directly to avoid poorly defined or incorrect elements in convoluted regions. Instead, the projections were established by the intersections of two cross-sectional planes and the brain surface with the plane normal directions determined by the initial nodal location relative to the brain surface (e.g., see Fig. 3bc). The automatic operation of the meshing scheme was maintained because no manual effort is involved in placing the boundary nodes. The details of developing the atlas mesh through a meshing script are secondary to the scope of this paper. A pseudo algorithm illustrating important steps involved in a typical meshing script is provided here for reference:

1. Initialize parameters for center and dimensions based on input geometry.
2. Create a multi-block and remove unnecessary corner blocks (e.g., Fig. 3a).
3. Sub-divide geometry and create internal surfaces/edges for nodal projections.
4. Project nodes onto the input surface and internal surfaces/edges (e.g., Fig. 3bc).
5. Spatially merge nodes along common boundaries and adjust mesh resolution (e.g., Fig. 3d).
6. Output the resulting mesh.

Interested readers may refer to [19], [20] and [24] for more detailed examples. Fig. 3d shows the top view of the resulting atlas mesh after refinement.

2.3 Image registration

A rigid registration was performed to transform the subject-specific geometry into the coordinate system of the atlas MR image to allow execution of the meshing script. Mutual information (MI) was applied to maintain full automation of the process [21]. To maximize MI as an objective function with respect to six DOF transformational (3 translational and 3 rotational) parameters, we adopted a steepest gradient descent algorithm and a tri-linear partial volume distribution interpolation scheme implemented in the Insight Segmentation and Registration Toolkit (ITK, version 3.10; [25]). To reduce the computational cost, sub-sampling was applied to the moving image (10% of the image voxels were randomly selected for registration in this study, which typically resulted in a 10-fold speedup compared to using all of the voxels).

The resulting transformation was then used to map the subject's brain surface into the atlas space (i.e., the "intermediate geometry" in Fig. 1). Because the intermediate and atlas geometries were similar in shape, size and spatial position, the same meshing script was applied to the intermediate geometry. The resulting mesh was finally rigidly transformed back into the subject MR image space by inverting the registration transformation (Fig. 1).

2.4 Mesh quality assessment

We selected a commonly used mesh quality measure, scaled Jacobian [26], to quantify the resulting mesh quality. The scaled Jacobian is the minimum determinant of the Jacobian matrix evaluated at each corner and the center of an element, divided by the corresponding edge lengths [27]. This scalar measure is dimensionless and ranges from −1.0 to 1.0, where a value of 1.0 represents a unit cube while negative values indicate the corresponding elements are inverted (non-convex) and unacceptable for FE analysis. Elements are preferred to have scaled Jacobian values close to 1.0 for the best accuracy in analysis (>0.6 in practice). Values between 0.0 and 0.2 are considered poor because they may result in questionable accuracy in FE analysis in the corresponding regions [26]. For this study, we defined mesh quality to be satisfactory when at least 95% of the elements had a scaled Jacobian greater than 0.6.

2.5 Mesh accuracy assessment

We assessed mesh accuracy by quantifying the distance between mesh boundary elements and the corresponding anatomical geometry to measure the fidelity of the model representation. Mesh accuracy was defined as the average distance between centroids of mesh boundary elements relative to their closest point projections found on the geometrical surface used as the input to the meshing script. The algorithm to compute “closest point projection” was identical to the one used in resolving contact search between a master and slave surface when implementing a contact boundary condition [28]. Briefly, for each boundary element centroid, its closest node on the triangulated geometrical surface was computed along with its projection on all of the triangles that share the same closest node. The closest point projection was then defined as the projection point closest to the centroid enclosed by the corresponding triangle. When no projection point satisfied the criteria, the closest node, itself, was chosen as the closest point projection. Distances between the centroids and their closest point projections were computed to assess mesh accuracy. A mesh accuracy was defined to be satisfactory when the average distance was less than 0.1 mm for all boundary element centroids and at least 95% of all distance values were less than 0.5 mm.

3. Data analysis

The atlas mesh was first constructed, and subject-specific brain meshes for the remaining 10 subjects were generated subsequently following the meshing scheme described. Multithreading (two quad cores or 8 processing units in total) was employed when performing the image-based rigid registration between the subject and atlas MR images and the computational cost in terms of execution time is reported. For all meshes created in this study, we report mesh quality and accuracy in terms of scaled Jacobian and surface distance, respectively. All data analyses were performed through MATLAB, and all computations were executed on an Intel Xeon computer running Windows Vista (2.00GHz, 8GB RAM).

4. Results

The average computational cost of all image-based registrations was 190 sec (from 156 to 245 sec; all converged within 200 iterations). Due to differences in head size and shape between the subject and atlas and because a rigid registration was used, some misalignment was evident (Fig. 4). However, the head *orientation* of all subjects aligned well with that of the atlas, which allowed the meshing script to be successfully executed using the segmented brain surface from each subject as input.

Two additional visualizations of the atlas mesh are shown in Fig. 5 to illustrate the distribution of mesh quality (see below for details). Subject-specific brain meshes were generated automatically (computational cost of approximately 5 sec) using the segmented brain surface transformed into the atlas space as the input for the meshing script (Fig. 6). All meshes were similar in topology and they had the same number of nodes and elements as those of the atlas (101.1 k and 97.8 k, respectively). Despite the varying brain morphology (size and shape) relative to the atlas (see Fig. 5b), all of the subject-specific meshes were generated successfully (i.e., no inverted elements).

Mesh quality was evaluated using the scaled Jacobian as shown in Figs. 5 and 6. The majority of elements had a scaled Jacobian close to 1.0. Elements with low values (e.g., <0.4) were in the basal region, especially around the temporal lobe and cerebellum interface. The vast majority of internal and boundary elements had a scaled Jacobian greater than 0.6 (99.5 ± 0.2% on average for all 11 subjects). Only a few had a value less than 0.2 (the number of elements ranged from 0 to 39 for the 11 meshes, representing less than 0.01% of the total number of elements on average). No element with a negative scaled Jacobian was found in any of the meshes generated. The minimum scaled Jacobian for each subject was typically within 0.1 to 0.2, and the smallest value across all subjects was 0.06 (subject 4). Mesh quality histogram distributions for the atlas mesh and a pool of the 10 subject-specific meshes are shown in Fig. 7.

Mesh accuracy was measured in terms of surface distance between the boundary elements and the geometrical surface as shown in Figs. 8 and 9. Most elements had a distance close to zero, although a few large values (>0.8 mm) were found near the cerebellum. For the atlas mesh, the average distance was 0.07 ± 0.10 mm with 0.61% of the distances greater than 0.5 mm (maximum distance of 1.8 mm). For the pool of 10 subject-specific meshes, the average distance was 0.07 ± 0.11 mm with 0.88% of the distances greater than 0.5 mm (maximum distance of 2.6 mm). Mesh accuracy histograms for the atlas and subject-specific meshes are shown in Fig. 10.

5. Discussion

Rapidly generating subject-specific meshes is important for evaluating the predictive capability of computational models on a large scale to improve and optimize personalized diagnosis and clinical treatment. To meet this need, we developed and validated a subject-specific, hexahedral mesh generator that maintains the same level of mesh quality and accuracy as an atlas mesh without the need for mesh repair. The mesh generator is completely automatic and computationally practical once an atlas mesh is developed. A meshing script is first created based on the segmented brain geometry of an atlas with a commercial meshing software package. For a given subject, the MR image volume is rigidly registered with the atlas and the segmented brain surface is transformed into the atlas space to allow the same meshing script to be executed. Because the registration is rigid, no mesh distortion or degradation in mesh quality is involved, which eliminates the need for mesh repair after the mesh is transformed back into the subject's space (see Fig. 1). Consequently, the same level of mesh quality is expected in subject-specific meshes relative to the atlas (the percentage of distorted elements was less than 0.01% for all of the 10 subjects tested). The percentage of distorted elements is often much higher with other mesh-matching techniques (e.g., 5–15% using mesh-matching without mesh repair for the femur [15]; 6.1% (4.9%) using mesh-matching with mesh repair for the femur (face) [18]; 6.5–10.6% using deformable registration when meshing the phalanx bones [17]; and 0.05% and 0.02% using automated wrapping and manual landmarks, respectively, when meshing the vertebra [16]).

The average distance between the mesh boundary elements and the geometrical image surface was 0.07 mm for all subjects and less than 1% of the distances were greater than 0.5 mm, demonstrating satisfactory mesh accuracy with our technique. The surface distance in our study was slightly larger than that reported in [17] (<0.05 mm) because we used the boundary element *centroids* instead of the boundary nodes for evaluation (the meshing software would enforce the boundary nodes to project onto the geometrical surface, leading to an average distance of 0.0015 mm, a non-zero value due to round-off errors). Interestingly, elements contributing to relatively poorer mesh quality and accuracy were found to occur in the same basal region of the brain (see Figs. 5, 6, 8, and 9), which is not surprising because of the greater changes in surface curvature in this region [19]. Increasing mesh density may reduce the ratio of elements with poorer mesh quality. However, the optimal mesh density is case-dependent because both simulation accuracy and cost have to be considered (all meshes developed in this study were successfully employed in dynamic impact simulations (duration of ~40 ms) with sufficient accuracy and acceptable computational cost (typically within 4 hours)). Nevertheless, our meshing scheme maintains the same level of mesh quality and accuracy relative to the atlas mesh and is completely automatic because of the automated brain segmentation, image registration, and mesh scripting.

A dedicated meshing script must be created similarly with other mesh-matching methods [5, 6, 8, 15, 16, 17, 18], which is a limitation of the current approach. The meshing script is essential to the success of the meshing scheme as well as to ensuring sufficient mesh quality. This task, however, is not trivial and requires significant effort especially when the geometry is complex (e.g., it took a few weeks to develop and optimize the meshing script used in this study; also, see [18] and [20] for examples of meshing the femur and heart ventricle, respectively). In addition, the meshing script may not be universally applicable and may need to be developed each time the anatomical morphology differs significantly. The level of anatomical detail in the mesh (e.g., inclusion of the falx when meshing the brain) is also directly related to the sophistication of the meshing script and our technique is able to generate meshes of geometrically complex anatomies.

Similarly to previously reported mesh-matching methods, registration plays an important role. However, our approach differs significantly from other techniques in that the registration was performed between subject and atlas MR images instead of matching the atlas mesh directly with the subject anatomy. Therefore, no mesh distortion is involved that leads to degradation in mesh quality, suggesting that our approach is likely to be more efficient than other methods because no additional mesh repair is required to correct for element regularity and quality [18]. Although *image*-based registration was employed in this study, surface-based registration (e.g., using the iterative closest point (ICP) algorithm [29]) can also be applied when only anatomical surfaces are available. However, image-based (especially intra-modality) registration is usually preferred because of its enhanced registration robustness and accuracy compared with surface-based approaches.

The combined computational cost of image registration and meshing was less than 4 minutes, whereas the computational cost for brain segmentation depends on the algorithm used and the desired level of segmentation detail. For example, performing a sophisticated sub-cortical segmentation requires 35–45 min using FreeSurfer [30] (by comparison, 5–10 min using FSL in this study). Sub-cortical segmentation is useful when classification of mesh elements is desired to characterize the corresponding sub-regions with different material properties.

The automated subject-specific mesh generator can also be employed to mesh other anatomical structures with an appropriate meshing script based on the input geometry, since

no constraints on the type of anatomy or anatomical morphology are imposed. In this work, we used a rigid registration between subject and atlas MR images because their head sizes and shapes were similar (see Fig. 4). When a subject's anatomy differs considerably in size but not in shape relative to the atlas, linearly scaling the subject anatomy to match the size of the atlas before applying the rigid registration is recommended. The resulting mesh can then be inversely scaled afterwards, in which case no mesh repair is necessary because no mesh distortion or degradation in mesh quality is involved. When a subject's anatomy differs significantly in shape compared with the atlas (e.g., infant brain vs. adult brain), the meshing script for the atlas may not be readily applicable or may result in undesirable mesh quality. As an alternative to revising the meshing script to account for differences in shape, a nonrigid registration can be useful to first register the subject and atlas MR image volumes before executing the meshing script. In this case, however, mesh distortion may occur that would degrade mesh quality, and additional mesh repair may be necessary. The performance of the approach when incorporating nonrigid registration in terms of the resulting mesh quality, accuracy, and computational efficiency warrants further investigation.

Finally, it is important to note that mesh quality not only influences the accuracy of FE analysis, but is also directly related to the simulation efficiency when a transient analysis is performed because a stable time increment is proportional to the smallest characteristic element dimension in the mesh [3]. Although the number of elements with low scaled Jacobian values (i.e., less than 0.2) is less than 0.01% which may not significantly influence the overall *accuracy* of a simulation, the existence of distorted elements may still lead to a substantial increase in the *computational cost* of a transient analysis. Consequently, further improvements in mesh quality are important and can likely be achieved by optimizing the initial topology of the brain geometry when developing the meshing script ([24]; see for example, [31], for different topologies applicable to meshing the brain). In this paper, we applied a simple topology and focused our effort on developing a meshing scheme to generate subject-specific meshes automatically. Fortunately, optimizing the meshing script in the future does not alter the subject-specific meshing scheme, which once again highlights the flexibility of our overall meshing approach.

In summary, we have developed an automated mesh generator for subject-specific, hexahedral meshes based on an existing atlas mesh that was produced using a dedicated meshing script. Using a pool of 11 subjects, we have demonstrated that the performance of the meshing technique is satisfactory in terms of both mesh quality and accuracy, and is computationally practical. In addition, the meshing technique is flexible because different anatomical structures or different levels of anatomical details can be incorporated through an appropriate meshing script without altering the overall meshing scheme. As a result, we believe that our meshing technique is potentially of significant interest to the biomechanical research community to aid in the construction of subject-specific, hexahedral meshes for a variety of anatomical structures.

Acknowledgments

This research was supported in part by William H. Neukom 1964 Institute for Computational Science at Dartmouth College, NIH grants R01HD048638, RO1NS055020, and CDC grant R01CE001254.

References

1. Cebral JR, Löhner R. From medical images to anatomically accurate finite element grids. Int J Numer Meth Eng. 2001; 51:985–1008.
2. Benzley, SE.; Perry, E.; Merkley, K.; Clark, B.; Sjaardama, G. A comparison of all hexahedral and all tetrahedral finite element meshes for elastic and elastoplastic analysis. Proceedings of the 4th international Meshing Roundtable; New Mexico: Sandia National Laboratories; 1995.

3. ABAQUS. Analysis User's Manual. Version 6.8. USA: Hibbitt, Karlsson and Sorensen; 2008.
4. Anderson AE, Peters CL, Tuttle BD, Weiss JA. Subject-Specific Finite Element Model of the Pelvis: Development, Validation and Sensitivity Studies. J Biomech Eng. 2005; 127(3):364. [PubMed: 16060343]
5. Sigal IA, Yang H, Roberts MD, Downs JC. Morphing methods to parameterize specimen-specific finite element model geometries. Journal of Biomechanics. 2010; 43(2):254–262. [PubMed: 19878950]
6. Castellano-Smith A, Hartkens T, Schnabel J, Hose D, Liu H, Hall W, Truwit C, Hawkes D, Hill D. Constructing patient specific models for correcting intraoperative brain deformation. Lecture Notes in Computer Science. 2001; 2208:1091–1098.
7. Taylor CA, Figueroa CA. Patient-specific modeling of cardiovascular mechanics. Annu Rev Biomed Eng. 2009; 11:109–34. [PubMed: 19400706]
8. O'Reilly MA, Whyne CM. Comparison of computed tomography based parametric and patient-specific finite element models of the healthy and metastatic spine using a mesh-morphing algorithm. Spine. 2008; 33:1876–81. [PubMed: 18670341]
9. Southern J, Pitt-Francis J, Whiteley J, et al. Multi-scale computational modelling in biology and physiology. Prog BiophysMol Biol. 2008; 96:60–89.
10. Portnoy S, Yizhar Z, Shabshin N, et al. Internal mechanical conditions in the soft tissues of a residual limb of a transtibial amputee. J Biomech. 2008; 41:1897–909. [PubMed: 18495134]
11. Cattaneo PM, Dalstra M, Melsen B. Strains in periodontal ligament and alveolar bone associated with orthodontic tooth movement analyzed by finite element. Orthod Craniofac Res. 2009; 12:120–8. [PubMed: 19419455]
12. Fuentes D, Oden JT, Diller KR, et al. Computational modeling and real-time control of patient-specific laser treatment of cancer. Ann Biomed Eng. 2009; 37:763–82. [PubMed: 19148754]
13. Neal ML, Kerckhoffs R. Current progress in patient-specific modeling. Brief Bioinform. 2010; 11:111–126. [PubMed: 19955236]
14. Kraus MF, Susmaras T, Caughlin BP, Walker CJ, Sweeney JA, Little DM. White matter integrity and cognition in chronic traumatic brain injury: a diffusion tensor imaging study. Brain. 2007; 130(10):2508–2519. [PubMed: 17872928]
15. Couteau B, Payan Y, Lavallee S. The mesh-matching algorithm: an automatic 3D mesh generator for finite element structures. J of Biomechanics. 2000; 33:1005–1009.
16. Sigal IA, Hardisty MR, Whyne CM. Mesh-morphing algorithms for specimen-specific finite element modeling. J of Biomechanics. 2008; 41:1381–1389.
17. Grosland NM, Bafna R, Magnotta V. Automated hexahedral meshing of anatomic structures using deformable registration. Computer Methods in Biomechanics and Biomedical Engineering. 2009; 12(1):35–43. [PubMed: 18688764]
18. Bucki M, Lobos C, Payan Y. A fast and robust patient specific Finite Element mesh registration technique: Application to 60 clinical cases. Medical Image Analysis. 2010; 14:303–317. [PubMed: 20299273]
19. Schonning A, Oommen B, Ionescu I, Conway T. Hexahedral mesh development of free-form formed geometry: The human femur exemplified. Computer-Aided Design. 2009; 41:566–572.
20. Wenk JF, Wall ST, Peterson RC, Helgerson SL, Sabbah HN, Burger M, Stander N, Ratcliffe MB, Guccione JM. A method for automatically optimizing medical devices for treating heart failure: designing polymeric injection patterns. J of Biomech Eng. 2009; 131(12):121011. [PubMed: 20524734]
21. Maes F, Collignon A, Vandermeulen D, Marchal G, Suetens P. Multimodality image registration by maximization of mutual information. IEEE Trans Med Imaging. 1997; 16(2):187–198. [PubMed: 9101328]
22. Greenwald RM, Gwin JT, Chu JJ, Crisco JJ. Head impact severity measures for evaluating mild traumatic brain injury risk exposure. Neurosurgery. 2008 Apr; 62(4):789–98. discussion 798. [PubMed: 18496184]
23. Woolrich MW, Jbabdi S, Patenaude B, Chappell M, Makni S, Behrens T, Beckmann C, Jenkinson M, Smith SM. Bayesian analysis of neuroimaging data in FSL. NeuroImage. 2009; 45:S173–186. [PubMed: 19059349]

24. TrueGrid User's Manual, Version 2.3. XYZ Scientific Applications, Inc;
25. Insight Segmentation and Registration Toolkit (ITK). http://www.itk.org/
26. Shepherd J, Dewey M, Woodbury A, Benzley S, Staten M, Owen S. Adaptive mesh coarsening for quadrilateral and hexahedral meshes. Finite Elements in Analysis and Design. 2010; 46(1–2):17–32.
27. Knupp PM. Algebraic mesh quality metrics. SIAM J Sci Comput. 2001; 23(1):193–218.
28. Ji S, Roberts DW, Hartov A, Paulsen KD. Brain-skull contact boundary condition in an inverse computational model. Medical Image Analysis. 2009; 13(4):659–672. [PubMed: 19560393]
29. Besl PJ, McKay ND. A Method for Registration of 3-D Shapes. IEEE Transactions on Pattern Analysis and Machine Intelligence. 1992; 14(2):239–256.
30. Fischl B, Salat DH, van der Kouwe AJW, Makris N, Ségonne F, Dale AM. Sequence-independent segmentation of magnetic resonance images. NeuroImage. 2004; 23(Suppl 1):S69–84. [PubMed: 15501102]
31. Horgan, TJ. A finite element model of the human head for use in the study of pedestrian accidents. National University of Ireland; 2005.

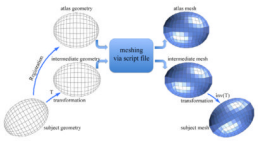

Fig. 1.

Illustration of the subject-specific meshing scheme. To generate a subject-specific mesh, the corresponding geometry is registered with the atlas and transformed into the atlas coordinate system in order to apply the meshing script. The resulting mesh is then transformed back into the subject coordinate system.

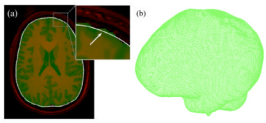

Fig. 2.

(a) Composite overlay of the segmented brain (green) and the corresponding axial MR image (red). (b) Smoothed outer boundary surface to be imported as a polygonal surface. Surface smoothing is evident when comparing the cross-section of the polygonal surface intersected by the axial imaging plane and the segmented brain (see arrow in inset in (a)).

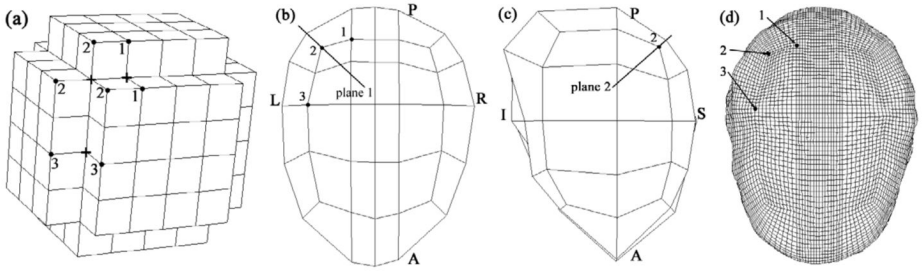

Fig. 3.

Illustration of the multi-block approach for meshing the atlas brain (a). Points with identical labels are projected to the same physical locations as shown in the coarse (b, c) and refined (d) meshes. Projection of the corner nodes (e.g., points labeled with “2”) on the brain surface is determined by the intersection of two cross-sectional planes and the brain surface (b, c).

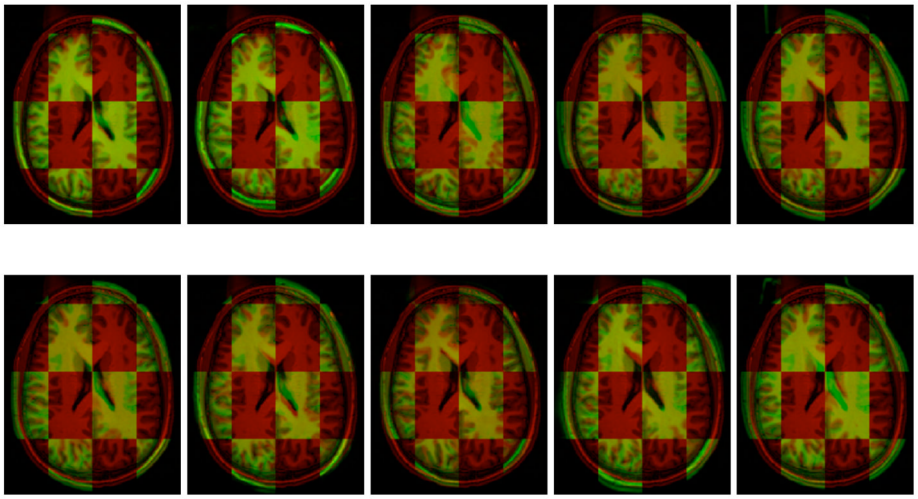

Fig. 4.

Checkerboard overlays of the 10 subjects (green) and atlas (red) MR axial images after rigid registration. Slight misalignments were due to differences in head size and shape resulting from rigid registration of the subject and atlas. These misalignments did not influence subject-specific mesh generation using the same meshing script.

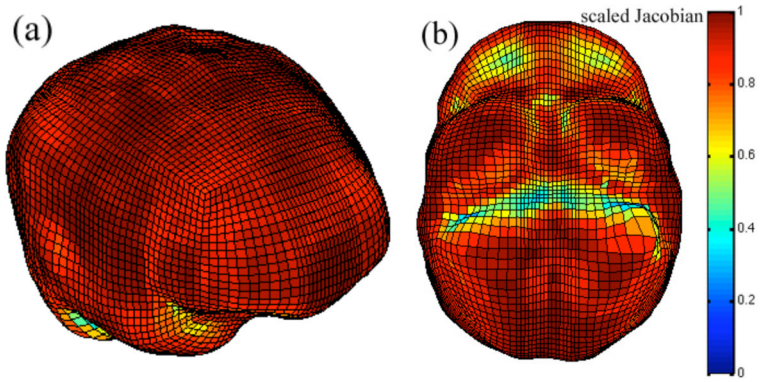

Fig. 5.
Color-coded distribution of scaled Jacobian for the atlas mesh in iso-view (a) and viewed from inferior to superior (b).

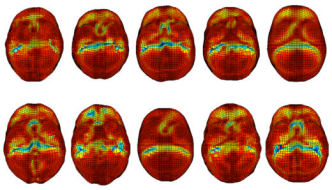

Fig. 6.
The 10 subject-specific, hexahedral brain meshes viewed from inferior to superior, showing the distribution of scaled Jacobian on the boundary elements. Color map scale identical to Fig. 5.

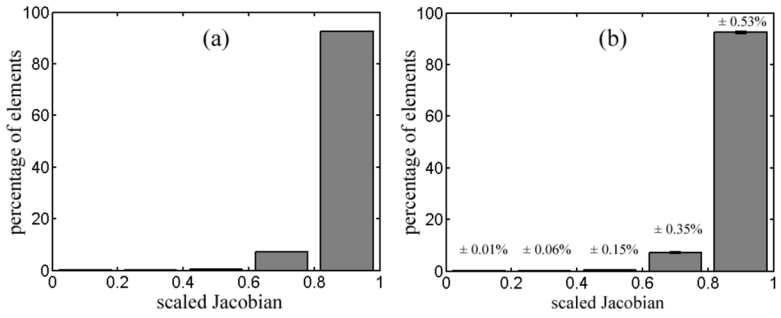

Fig. 7.

Histograms of scaled Jacobian for the atlas mesh (a) and the pool of 10 subject-specific meshes (b). Standard deviations for the subject-specific statistics are also reported.

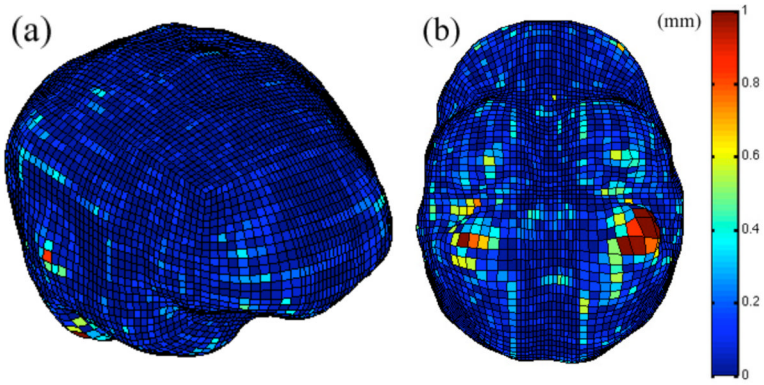

Fig. 8.
Surface distance for the atlas mesh in iso-view (a) and viewed from inferior to superior (b). Distances >1 mm were capped to 1.0 mm for ease of visualization.

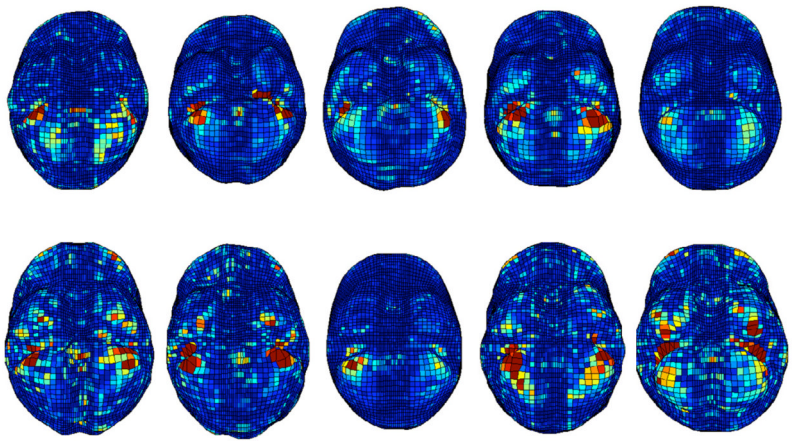

Fig. 9.

Surface distance for the 10 subject-specific meshes viewed from inferior to superior (distances >1 mm were capped to 1.0 mm for ease of visualization). Color map scale identical to Fig. 8.

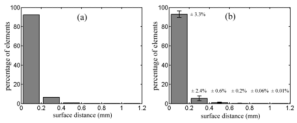

Fig. 10.

Histograms of surface distance for the atlas mesh (a) and the pool of 10 subject-specific meshes (b). Standard deviations for the subject-specific statistics are also reported. Distances >1 mm were lumped into a single bin from 1 to 1.2 for ease of visualization.